Supporting Information for

Hollow N-doped carbon nanofibers bring superior potassium-storage performance

Ya Ru Pei, Ming Zhao, Hong Yu Zhou, Chun Cheng Yang*, Qing Jiang

Key Laboratory of Automobile Materials (Jilin University), Ministry of Education, and School of Materials Science and Engineering, Jilin University, Changchun 130022, China

* Corresponding author. Tel.: +86-431-85095371; Fax: +86-431-85095876; E-mail: ccyang@jlu.edu.cn (C. C. Yang).

† Electronic Supplementary Information (ESI) available. See DOI: 10.1039/x0xx00000x

Supplementary Note

Electrochemical performances of HNCNFs-700 in sodium-ion batteries (SIBs)

Electrochemical measurements

The electrochemical Na-storage performances of HNCNFs-700 were also investigated using coin-type (CR2025) half-cell configurations *vs.* Na metal as the counter electrode, which were assembled in an Ar-filled glove box ([O_2]<1 ppm, [H_2O]<1 ppm). The separator was Whatman glass fiber (GF/D) and the electrolyte was the mixture of ethylene carbonate and diethyl carbonate with a volume ratio of 1:1, containing 1 M $NaClO_4$ and 5 wt% fluoroethylene carbonate. The working electrodes were fabricated by mixing 70 wt% HNCNFs-700, 20 wt% conductive agent (Super P) and 10 wt% binder (Na-CMC) using deionized water as the solvent. The obtained slurry was pasted uniformly on Cu foil and dried in vacuum at 70 °C for 12 h. Then the electrodes were cut into discoidal pieces with a diameter of 12 mm and the mass loading of active materials is 0.4-0.6 mg cm^{-2}. Galvanostatic charge/discharge cycling tests were performed using a LAND CT2001A battery testing system in the voltage range of 0.01-3 V (*vs.* Na^+/Na). Cyclic voltammetry (CV) measurements were carried out on an Ivium-n-Stat electrochemical workstation (Ivium Technologies) with a potential scan rate of 0.1 mV s^{-1} between 0.01-3.0 V (*vs.* Na^+/Na).

Electrochemical performances

The electrochemical performances of HNCNFs-700 as an anode in SIBs are shown in Fig. S14. CV curves of the HNCNFs-700 electrodes were measured at a

scan rate of 0.1 mV s^{-1} within 0.01-3.0 V (*vs.* Na^+/Na) (see Fig. S14a). The broad reduction peak at approximately 0.5 V in the first scan, which disappears at the subsequent scans, can be ascribed to the formation of SEI films. The sharp reversible cathodic peak close to 0.01 V as well as the wide anodic peak are related to the intercalation and deintercalation of Na^+ into/from carbon matrix, respectively. During the following cycles, two broad peaks around 1.2 V and 0.8 V are attributed to the interaction of Na^+ into species of N atoms. The CV curves from the second cycle to the fifth cycle are well overlapped, which demonstrates an excellent reversibility of the HNCNFs-700 electrode. Fig. S14b shows the galvanostatic charge/discharge voltage profiles of the HNCNFs-700 electrode for the 1^{st}, 2^{nd}, 50^{th}, 100^{th} and 200^{th} cycles at 0.1 A g^{-1}. The initial discharge and charge capacities are 788.6 and 345.4 mAh g^{-1}, respectively, corresponding to an initial CE of 43.8%. The HNCNFs-700 electrode delivers a reversible capacity of 308.3 mAh g^{-1} after 200 cycles with CE close to 100% (see Fig. S14c). The HNCNFs-700 electrode also shows superior rate performance with reversible capacities of 323.7, 278.6, 245.9, 229.8, 218.2, 209.6, 188.3 and 169.5 mAh g^{-1} at 0.1, 0.2, 0.4, 0.6, 0.8, 1, 2 and 5 A g^{-1}, respectively (see Fig. S14d). When the current density switches back to 0.1 A g^{-1}, the HNCNFs-700 electrode recovers a specific capacity of 300.8 mAh g^{-1} rapidly and then remains stable for further cycling. Besides, the HNCNFs-700 electrode maintains a high reversible capacity of 223.2 mAh g^{-1} at 1 A g^{-1} after 5000 cycles with CE close to 100% (see Fig. S14e). This suggests HNCNFs-700 is also an excellent anode material for SIBs.

The Na-storage behavior of the HNCNFs-700 electrode was also analyzed by CV measurements at different scan rates from 0.2 to 1 mV s^{-1} (see Fig. S15a). The calculated *b* values for cathodic and anodic peaks are also both much closer to 1, indicating the Na-storage behavior is dominated by surface capacitive effect. The pseudocapacitive contributions of the HNCNFs-700 electrode at different scan rates are displayed in Fig. S15d.

Supplementary Figures

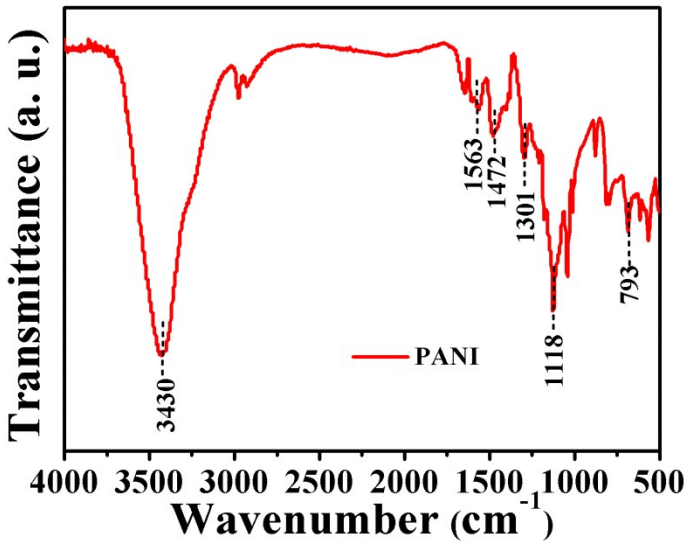

Fig. S1 FT-IR spectrum of PANI nanofibers.

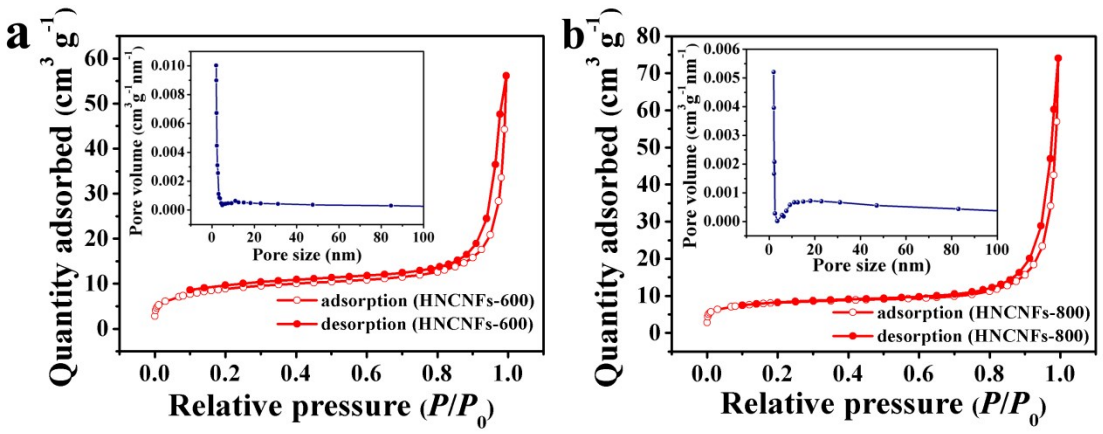

Fig. S2 N_2 adsorption/desorption isotherms and the corresponding pore size distribution (the inset) of (a) HNCNFs-600 and (b) HNCNFs-800.

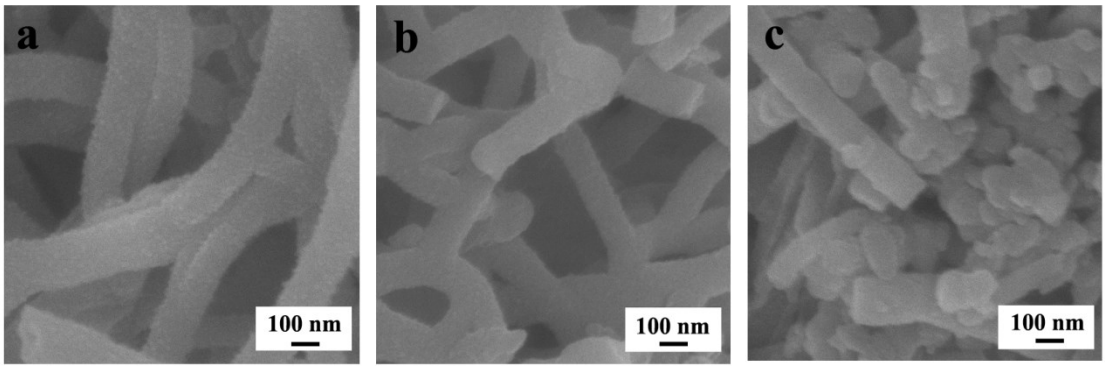

Fig. S3 SEM images of (a) PANI precursor, (b) HNCNFs-600, and (c) HNCNFs-800.

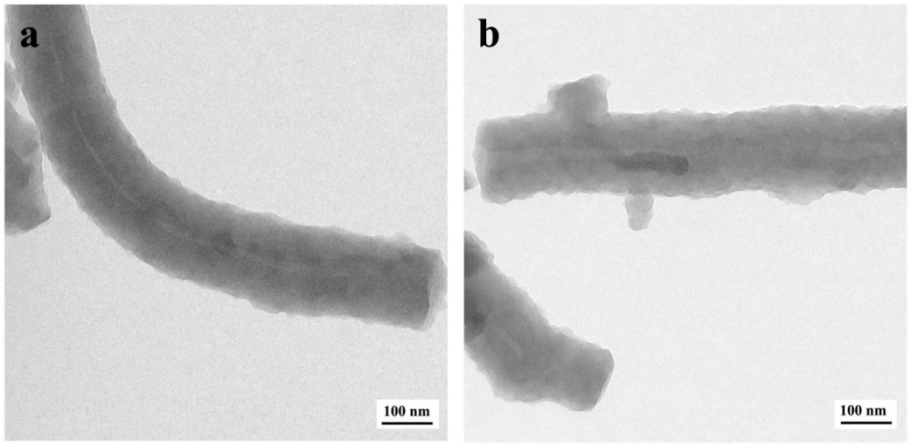

Fig. S4 TEM images of (a) HNCNFs-600 and (b) HNCNFs-800.

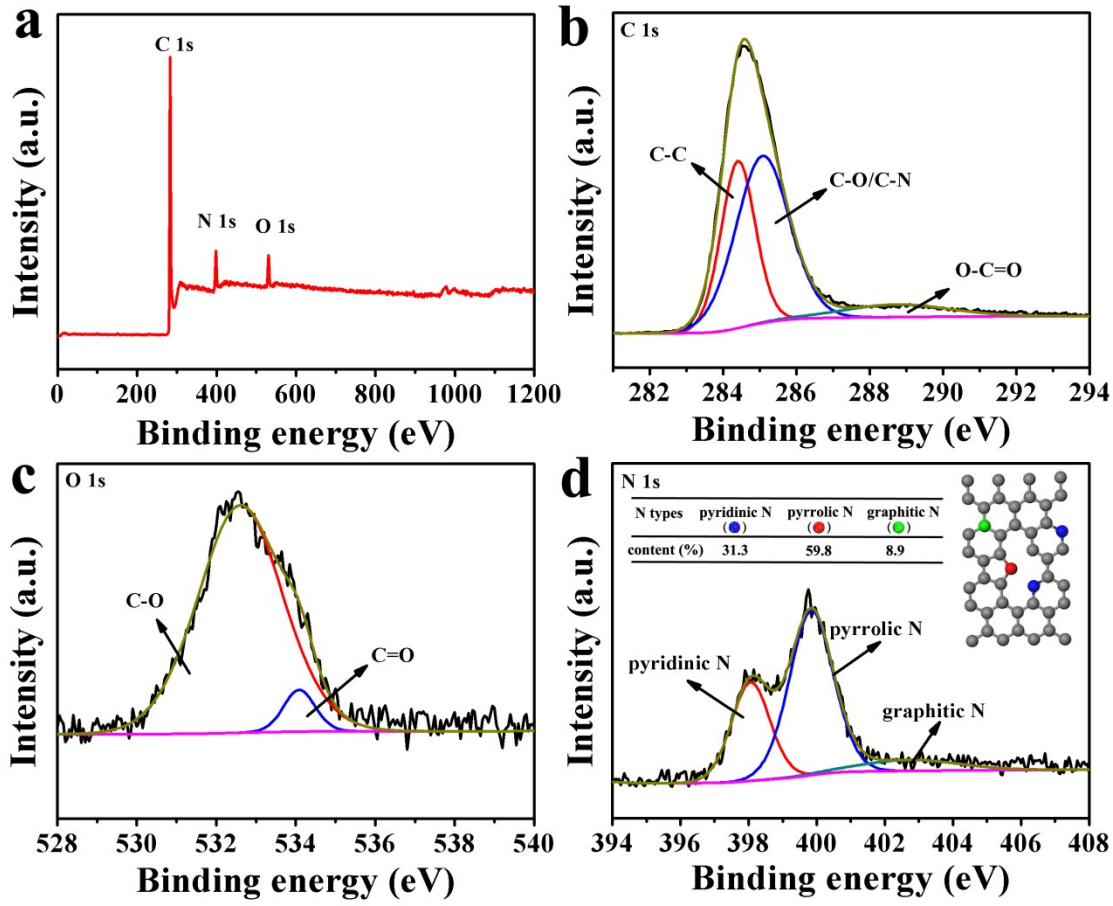

Fig. S5 (a) XPS survey spectrum of HNCNFs-600. (b), (c) and (d) are high-resolution XPS spectra of C 1s, O 1s and N 1s, respectively.

Fig. S6 (a) XPS survey spectrum of HNCNFs-800. (b), (c) and (d) are high-resolution XPS spectra of C 1s, O 1s and N 1s, respectively.

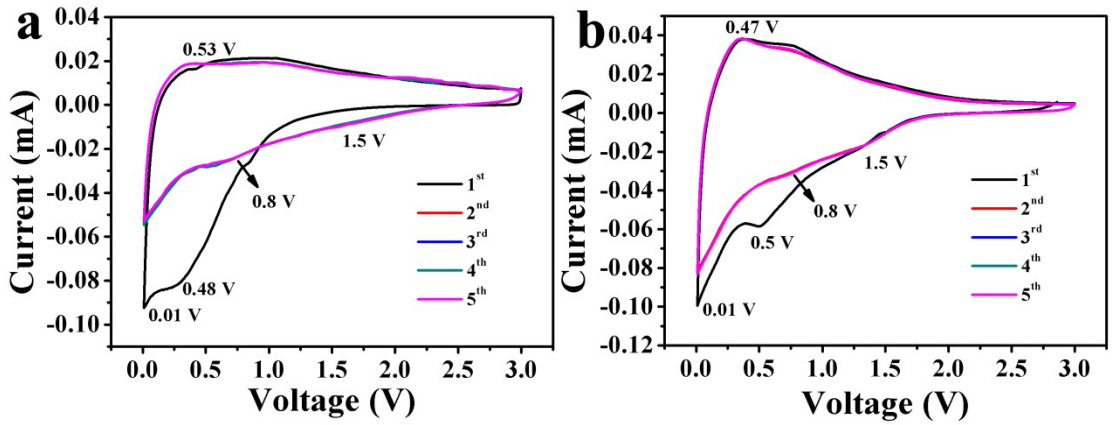

Fig. S7 CV curves of (a) HNCNFs-600 and (b) HNCNFs-800 electrodes at a scan rate of 0.1 mV s^{-1}.

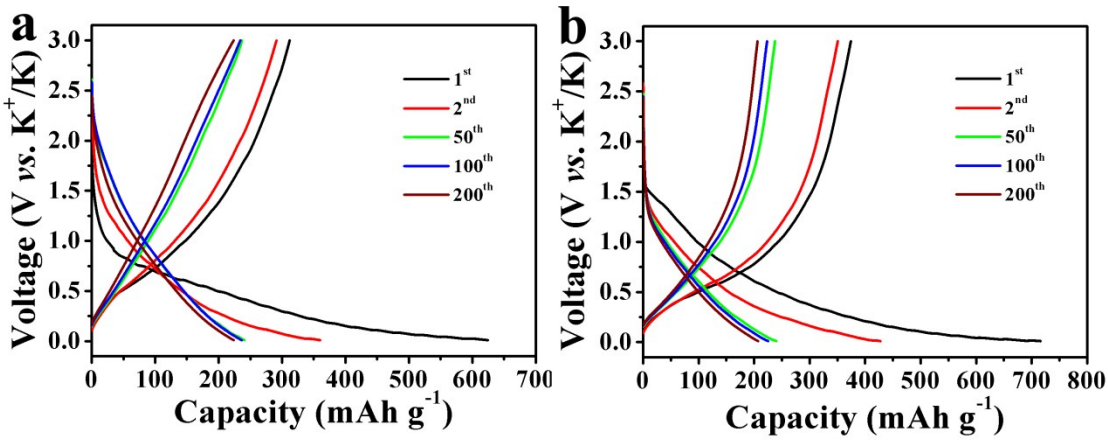

Fig. S8 Galvanostatic charge/discharge curves of (a) HNCNFs-600 and (b) HNCNFs-800 electrodes for the 1st, 2nd, 50th, 100th and 200th cycles at a current density of 0.1 A g^{-1}.

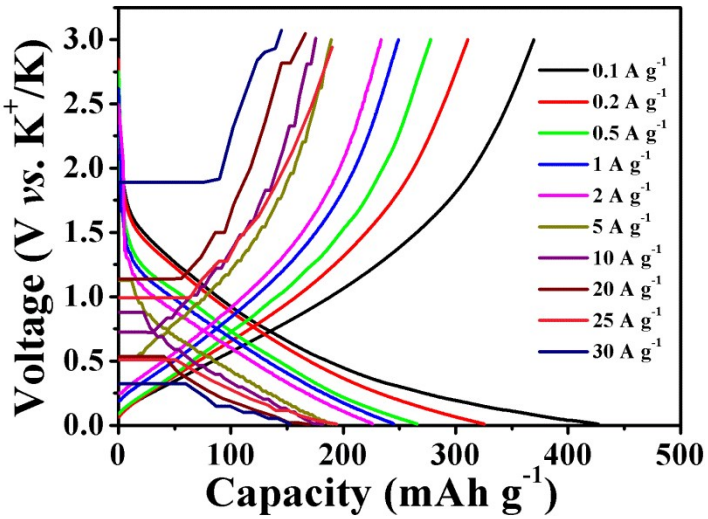

Fig. S9 Galvanostatic charge/discharge curves of the HNCNFs-700 electrode at various current densities.

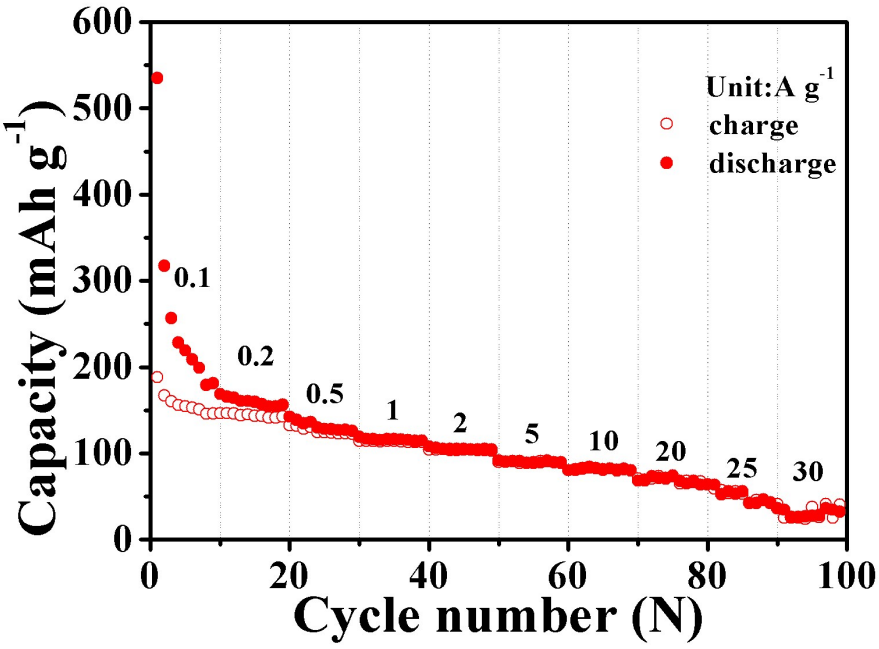

Fig. S10 Rate performance of the super P electrode at various current densities.

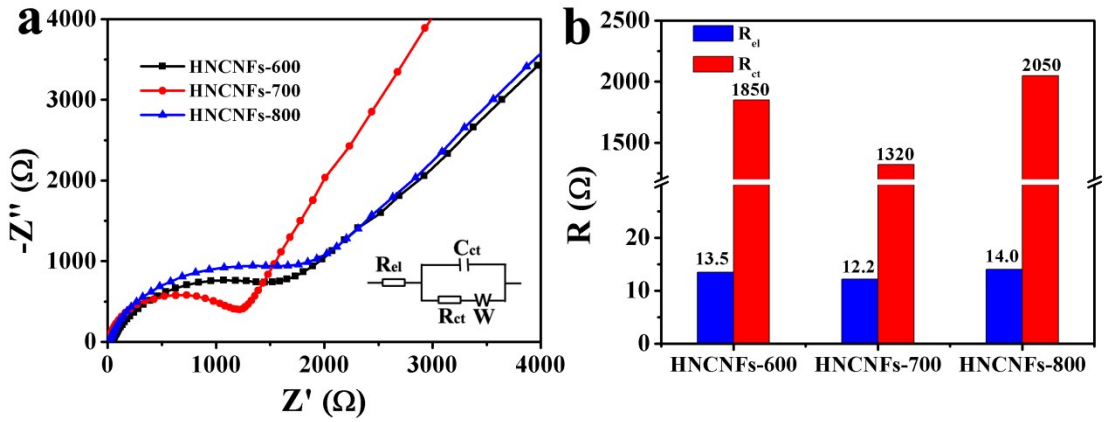

Fig. S11 (a) EIS of HNCNFs-600, HNCNFs-700 and HNCNFs-800 electrodes in fresh PIBs, where the inset shows the corresponding equivalent circuit diagram. (b) The electrolyte resistance (R_{el}) and charge transfer resistance (R_{ct}) values of HNCNFs-600, HNCNFs-700 and HNCNFs-800 electrodes.

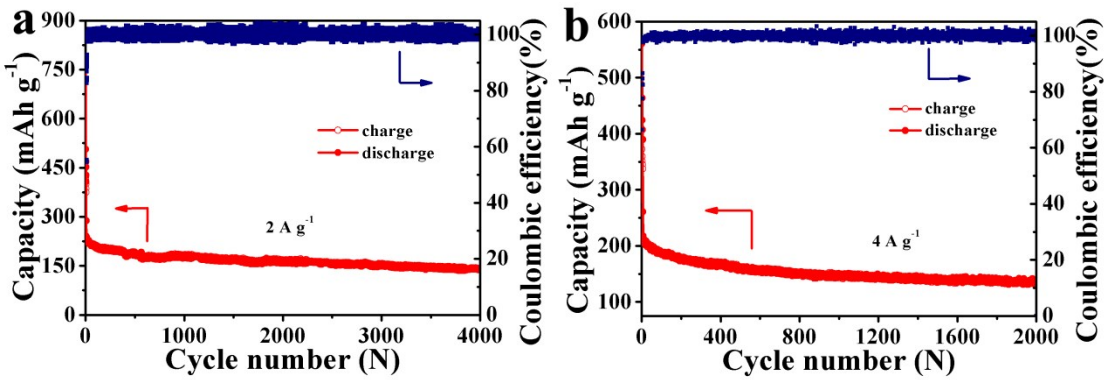

Fig. S12 Cycling performance of the HNCNFs-700 electrode as well as the coulombic efficiency at (a) 2 A g^{-1} for 4000 cycles and (b) 4 A g^{-1} for 2000 cycles.

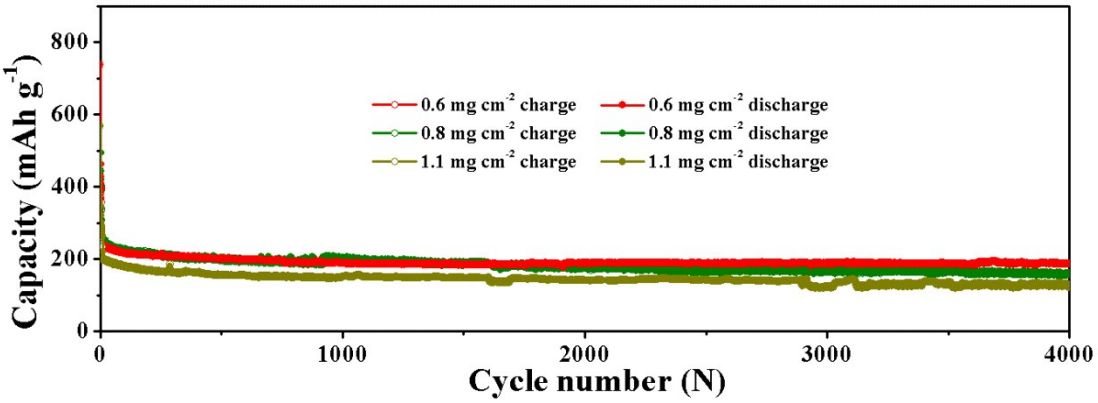

Fig. S13 Cycling performance of the HNCNFs-700 electrode with different mass loadings at 1 A g^{-1} for 4000 cycles.

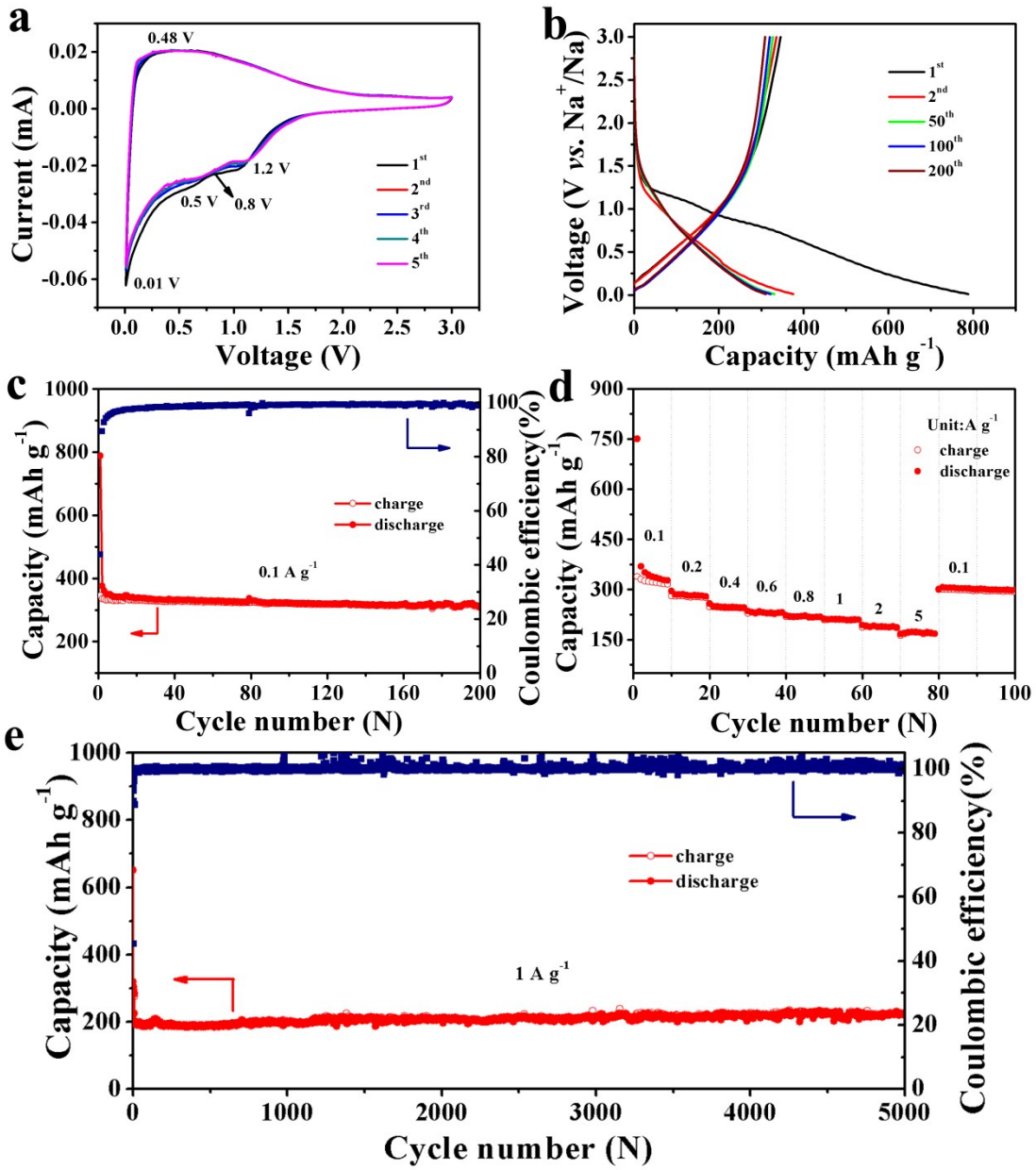

Fig. S14 Electrochemical performances of the HNCNFs-700 electrode in SIBs. (a) CV curves of the HNCNFs-700 electrode at a scan rate of 0.1 mV s^{-1}. (b) Galvanostatic charge/discharge curves of the HNCNFs-700 electrode for the 1st, 2nd, 50th, 100th and 200th cycles at 0.1 A g^{-1}. (c) Cycling performance of the HNCNFs-700 electrode as well as the coulombic efficiency at 0.1 A g^{-1}. (d) Rate performance of the HNCNFs-700 electrode at various current densities. (e) Long cycling performance of the HNCNFs-700 electrode as well as the coulombic efficiency at 1 A g^{-1}.

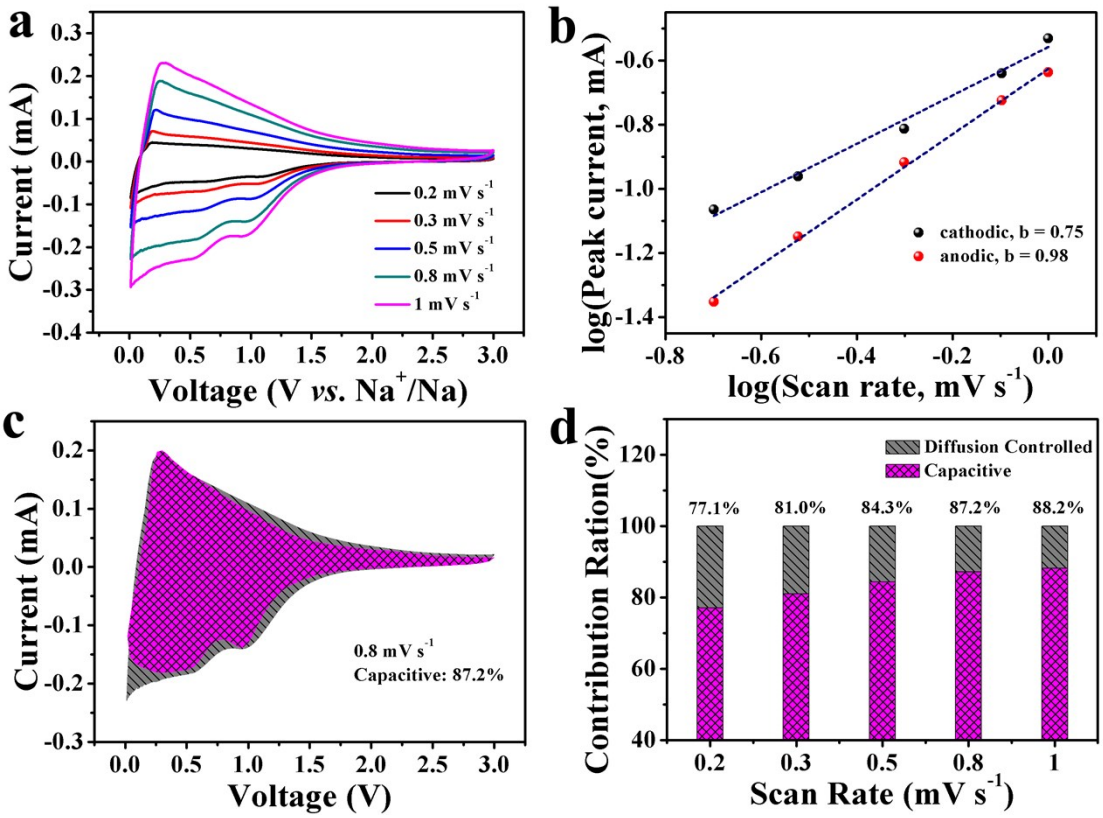

Fig. S15 Electrochemical kinetics analysis in SIBs. (a) CV curves of the HNCNFs-700 electrode at different scan rates from 0.2 to 1 mV s^{-1}. (b) Measurement of *b* value with the relationship between log(*i*) and log(*v*). (c) Capacitive and diffusion-controlled contributions to the charge storage at 0.8 mV s^{-1}. (d) Normalized contribution ratios of capacitive and diffusion-controlled capacities of the HNCNFs-700 electrode at different scan rates.

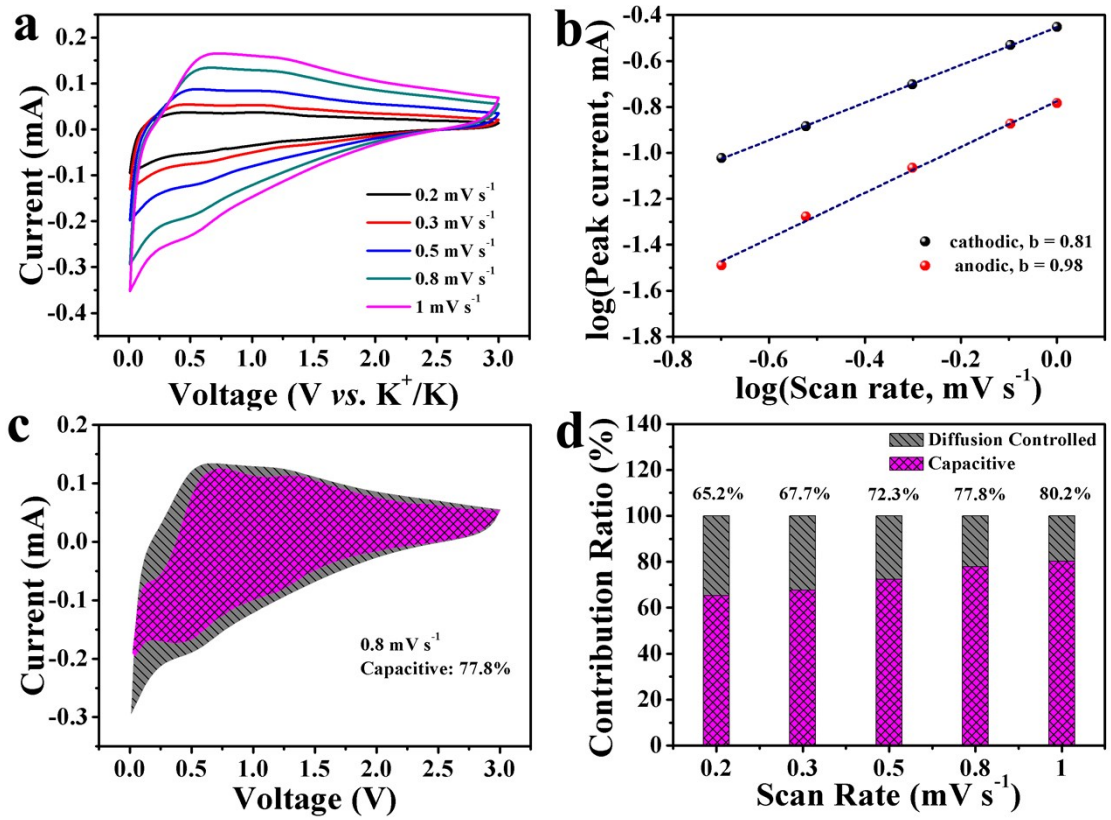

Fig. S16 Electrochemical kinetics analysis. (a) CV curves of the HNCNFs-600 electrode at different scan rates from 0.2 to 1 mV s^{-1}. (b) Measurement of *b* value with the relationship between log(*i*) and log(*v*). (c) Capacitive and diffusion-controlled contributions to the charge storage at 0.8 mV s^{-1}. (d) Normalized contribution ratios of capacitive and diffusion-controlled capacities of the HNCNFs-600 electrode at different scan rates.

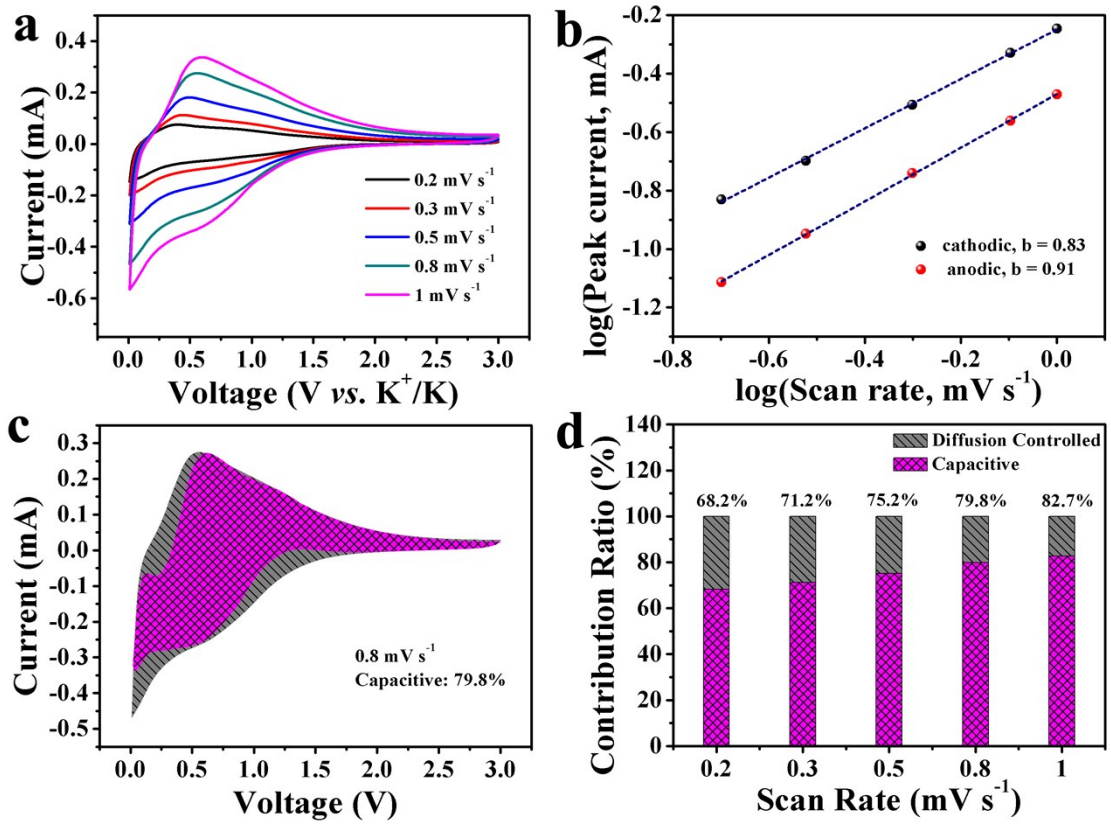

Fig. S17 Electrochemical kinetics analysis. (a) CV curves of the HNCNFs-800 electrode at different scan rates from 0.2 to 1 mV s^{-1}. (b) Measurement of *b* value with the relationship between log(*i*) and log(*v*). (c) Capacitive and diffusion-controlled contributions to the charge storage at 0.8 mV s^{-1}. (d) Normalized contribution ratios of capacitive and diffusion-controlled capacities of the HNCNFs-800 electrode at different scan rates.

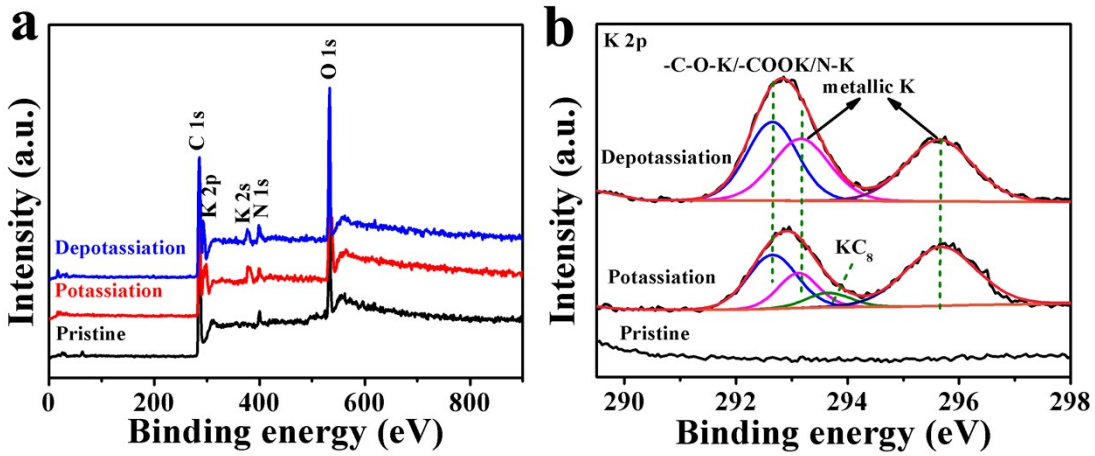

Fig. S18 *Ex-situ* XPS analysis. (a) XPS survey spectra of the HNCNFs-700 electrode under the pristine, potassiation and depotassiation states. (b) High-resolution XPS spectra of K 2p.

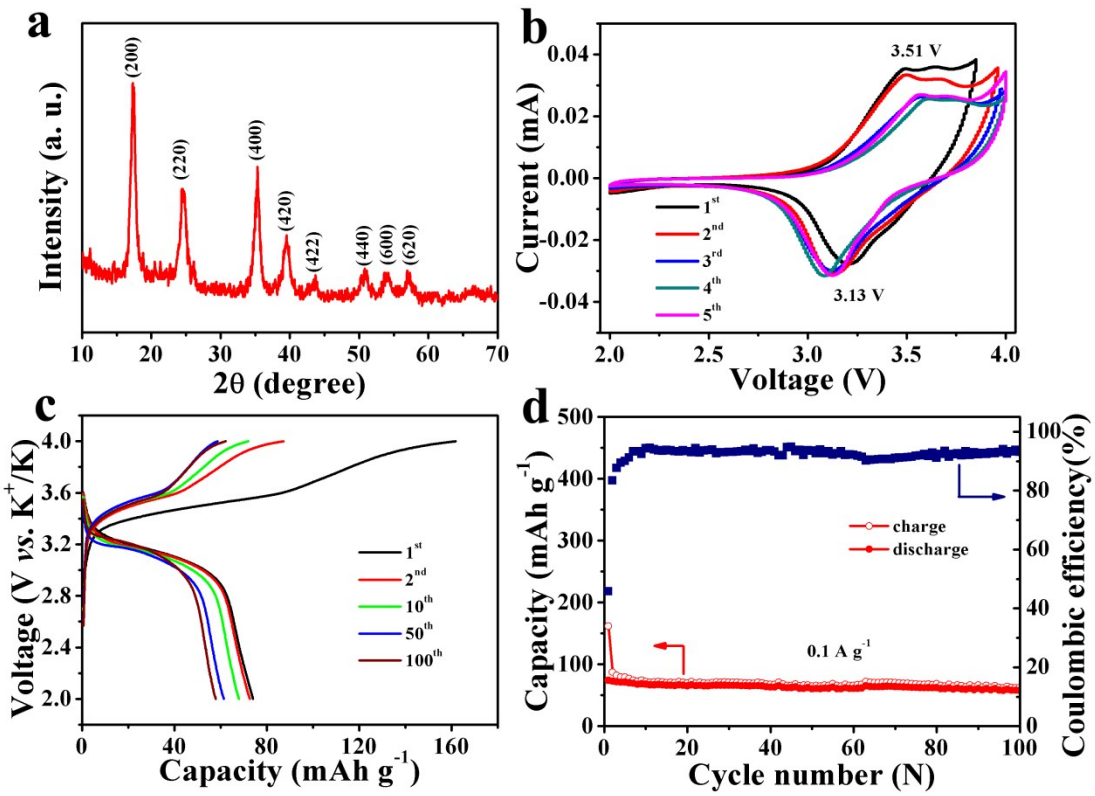

Fig. S19 Structural characterization and electrochemical performance of KPBNPs in a half cell. (a) XRD pattern. (b) CV curves of the KPBNPs electrode at a scan rate of 0.1 mV s^{-1}. (c) Galvanostatic charge/discharge curves of the KPBNPs electrode for the 1st, 2nd, 10th, 50th and 100th cycles at 0.1 A g^{-1}. (d) Cycling performance of the KPBNPs cathode as well as the coulombic efficiency at 0.1 A g^{-1}.

Supplementary Table

Table S1. Structure properties and surface chemistry of three different HNCNFs.

Materials	d_{002} (nm)	I_D/I_G	S_{BET} (m^2 g^{-1})	C (at.%)	N (at.%)	O (at. %)	% of total N 1s		
							pyridinic N	pyrrolic N	graphitic N
HNCNFs-600	0.416	1.67	29.6	84.5	10.3	5.2	31.3	59.8	8.9
HNCNFs-700	0.409	1.59	34.3	85.2	8.2	6.6	38.1	45.7	16.2
HNCNFs-800	0.401	1.42	26.1	88.3	7.4	4.3	31.7	44.9	23.4

Table S2. Electrochemical properties of three different HNCNFs.

Materials	Initial discharge/charge capacity (mAh g^{-1})	Initial CE (%)	Capacity (mAh g^{-1})[a]	Rate performance (mAh g^{-1})[b]	Cycling performance (mAh g^{-1})[c]	R_{ct} (Ω)
HNCNFs-600	624.7/312.1	49.9	223.2	121.6	60.5	1850
HNCNFs-700	781.9/410.6	52.5	274.5	139.7	188.4	1320
HNCNFs-800	715.6/374.2	52.3	206.4	70.3	89.5	2050

[a] Discharge capacities of the HNCNFs electrodes at 0.1 A g^{-1} after 200 cycles.

[b] Discharge capacities of the HNCNFs electrodes at 30 A g^{-1}.

[c] Discharge capacities of the HNCNFs electrodes after 4000 cycles at 1 A g^{-1}.

Table S3. Comparisons of electrochemical properties of some carbon-based electrode materials in PIBs reported in open literatures.

Materials	Initial CE	Rate performance	Cycling performance	Reference
HNCNFs-700	52.5%	239.6 mAh g^{-1} (2 A g^{-1}) 211.0 mAh g^{-1} (5 A g^{-1}) 190.2 mAh g^{-1} (10 A g^{-1}) 161.7 mAh g^{-1} (20 A g^{-1}) 139.7 mAh g^{-1} (30 A g^{-1})	274.5 mAh g^{-1} (200 cycles, 0.1 A g^{-1}) 188.4 mAh g^{-1} (4000 cycles, 1 A g^{-1}) 141.7 mAh g^{-1} (4000 cycles, 2 A g^{-1}) 132.5 mAh g^{-1} (2000 cycles, 4 A g^{-1})	This work
Necklace-like N-doped hollow carbon	~30%	224.3 mAh g^{-1} (1 A g^{-1}) 204.8 mAh g^{-1} (2 A g^{-1})	293.5 mAh g^{-1} (400 cycles, 0.2 A g^{-1}) 161.3 mAh g^{-1} (1600 cycles, 1 A g^{-1})	Ref. [18] of the text
3D N-doped framework carbon	24.3%	168 mAh g^{-1} (1 A g^{-1}) 146 mAh g^{-1} (2 A g^{-1}) 115 mAh g^{-1} (5 A g^{-1}) 111 mAh g^{-1} (10 A g^{-1})	137 mAh g^{-1} (1000 cycles, 2 A g^{-1})	[1]
N/O dual-doped carbon network	47.12%	205 mAh g^{-1} (1 A g^{-1}) 181 mAh g^{-1} (2 A g^{-1}) 175 mAh g^{-1} (5 A g^{-1})	260 mAh g^{-1} (100 cycles, 0.1 A g^{-1}) 160 mAh g^{-1} (4000 cycles, 1 A g^{-1})	Ref. [39] of the text
N-doped porous carbon	48.9%	185 mAh g^{-1} (10 A g^{-1})	384 mAh g^{-1} (500 cycles, 0.1 A g^{-1}) 226.1 mAh g^{-1} (1000 cycles, 1 A g^{-1}) 194 mAh g^{-1} (1000 cycles, 2 A g^{-1}) 160.5 mAh g^{-1} (1000 cycles, 5 A g^{-1})	Ref. [30] of the text
Highly N-doped carbon fibers	49%	153 mAh g^{-1} (2 A g^{-1}) 126 mAh g^{-1} (5 A g^{-1}) 104 mAh g^{-1} (10 A g^{-1}) 101 mAh g^{-1} (20 A g^{-1})	248 mAh g^{-1} (100 cycles, 0.05 A g^{-1}) 164 mAh g^{-1} (2000 cycles, 1 A g^{-1}) 146 mAh g^{-1} (4000 cycles, 2 A g^{-1})	Ref. [19] of the text
N/O dual-doped hierarchical porous hard carbon	25%	118 mAh g^{-1} (3 A g^{-1})	230.6 mAh g^{-1} (100 cycles, 0.05 A g^{-1}) 130 mAh g^{-1} (1100 cycles, 1050 mA g^{-1})	Ref. [29] of the text
Amorphous ordered mesoporous carbon	63.6%	144 mAh g^{-1} (1 A g^{-1})	257.4 mAh g^{-1} (100 cycles, 0.05 A g^{-1}) 146.5 mAh g^{-1} (1000 cycles, 1 A g^{-1})	Ref. [4] of the text
Ultra-high pyridinic N-doped porous carbon	20%	178 mAh g^{-1} (5 A g^{-1})	260 mAh g^{-1} (120 cycles, 0.05 A g^{-1}) 152 mAh g^{-1} (3000 cycles, 1 A g^{-1})	[2]
Free-standing porous carbon nanofibers paper	24.1%	190 mAh g^{-1} (2 A g^{-1}) 140 mAh g^{-1} (5 A g^{-1}) 100 mAh g^{-1} (7.7 A g^{-1})	270 mAh g^{-1} (80 cycles, 0.02 A g^{-1}) 211 mAh g^{-1} (1200 cycles, 0.2 A g^{-1})	Ref. [13] of the text

Table S4. The mass loadings of some carbon-based anodes in PIBs reported in open literatures.

Active materials	Mass loading (mg cm^{-2})	Cycling performance	Reference
HNCNFs-700	0.6	188.4 mAh g^{-1} (1 A g^{-1}, 4000 cycles) 141.7 mAh g^{-1} (2 A g^{-1}, 4000 cycles) 132.5 mAh g^{-1} (4 A g^{-1}, 4000 cycles)	This work
HNCNFs-700	0.8	161.2 mAh g^{-1} (1 A g^{-1}, 4000 cycles)	This work
HNCNFs-700	1.1	130.4 mAh g^{-1} (1 A g^{-1}, 4000 cycles)	This work
N-doped soft carbon frameworks	1.0	165 mAh g^{-1} (1 A g^{-1}, 500 cycles)	[3]
N/O dual-doped carbon network	0.8	160 mAh g^{-1} (1 A g^{-1}, 4000 cycles)	Ref. [44] of the text
N-doped carbon nanotubes	1.2	60 mAh g^{-1} (2 A g^{-1}, 1000 cycles)	[4]
N-doped framework carbon	0.7-1.0	137 mAh g^{-1} (2 A g^{-1}, 1000 cycles)	[5]
soft Carbon	1.0-1.5	200 mAh g^{-1} (20 mA g^{-1}, 100 cycles)	[6]
N/S codoped carbon microboxes	1.2	180 mAh g^{-1} (0.5 A g^{-1}, 1000 cycles)	Ref. [1] of the text
porous thin carbon shells	1.0-1.2	65 mAh g^{-1} (2 A g^{-1}, 900 cycles)	[7]
graphite foam	1.9	200 mAh g^{-1} (40 mA g^{-1}, 200 cycles)	[8]
carbon nanotubes-interweaved layer on graphite flakes	0.8	234.4 m Ah g^{-1} (2 A g^{-1}, 1500 cycles)	[9]
N/S co-doped porous carbon	1.2	125 mAh g^{-1} (1 A g^{-1}, 1000 cycles)	[10]
N-doped porous carbon	0.64	226.1 mAh g^{-1} (1 A g^{-1},1000 cycles)	Ref. [30] of the text
N-doped bamboo-like carbon nanotubes	0.5	204 mAh g^{-1} (0.5 A g^{-1}, 1000 cycles)	[11]
hollow carbon nanospheres	0.2	144.3 mAh g^{-1} (4 A g^{-1}, 2000 cycles)	Ref. [11] of the text

graphitic carbon nanocage	0.8-1.0	248 mAh g^{-1} (55 mA g^{-1}, 100 cycles)	Ref. [49] of the text
N-doped carbon nanotubes	0.7	102 mAh g^{-1} (2 A g^{-1}, 500 cycles)	[12]
few layer N-doped graphene	0.63-0.75	150 mAh g^{-1} (0.5 A g^{-1}, 500 cycles)	[13]
high pyridine N-doped porous carbon	0.8	231 mAh g^{-1} (0.5 A g^{-1}, 2000 cycles)	Ref. [15] of the text
amorphous ordered mesoporous carbon	1.0	146 mAh g^{-1} (1 A g^{-1}, 1000 cycles)	Ref. [4] of the text
highly N-doped carbon nanofibers	1.5	164 mAh g^{-1} (1 A g^{-1}, 2000 cycles)	Ref. [19] of the text
N-doped carbon nanofibers	0.9-1.3	103.4 mAh g^{-1} (0.5 A g^{-1}, 1000 cycles)	Ref. [41] of the text
expanded graphite	2.0	174 mAh g^{-1} (0.2 A g^{-1}, 500 cycles)	Ref. [43] of the text
highly disordered hard carbon	1.0	240 mAh g^{-1} (0.2 A g^{-1}, 150 cycles)	[14]
3D rGO aerogel	0.7-1.0	137 mAh g^{-1} (2 A g^{-1}, 1000 cycles)	[15]
N/O dual-doped hard carbon	0.9	130 mAh g^{-1} (1050 mA g^{-1}, 1100 cycles)	Ref. [29] of the text
hard-soft composite carbon	2.0	200 mAh g^{-1} (0.2 A g^{-1}, 200 cycles)	[16]
ultra-high pyridinic N-doped porous carbon	1.0	152 mAh^{-1} (1 A g^{-1}, 3000 cycles)	[2]
few-layer F-doped graphene foam	0.52-0.58	165.9 mAh g^{-1} (0.5 A g^{-1}, 200 cycles)	[17]

Table S5. Energy density (*E*) of carbon-based potassium-ion full cells reported in open literatures.

Materials	*E* (Wh kg^{-1})	Reference
HNCNFs-700//KPBNPs	70.3	This work
carbon foam//carbon foam	58	[18]
N-doped carbon nanotubes//laser scribed graphene	65	[4]
activated carbon//K_2TP	101	[19]
onion-like carbon//activated carbon	142	[20]
N, P-codoped graphene grown on carbon cloth//KPB	231.5	[21]
graphenic carbon//$K_2Ti_6O_{13}$	58.2	[22]
activated carbon//$Ca_{0.5}Ti_2(PO_4)_3$@C	80	[23]
graphite//prussian blue	110	Ref. [55] of the text
soft carbon//commercialized activated carbon	120	[24]
N-doped porous carbon// PTCDA	153	[2]

References

1 B. J. Yang, J. T. Chen, L. Y. Liu, P. J. Ma, B. Liu, J. W. Lang, Y. Tang and X. B. Yan, *Energy Storage Mater.*, 2019, **23**, 522-529.

2 Y. H. Xie, Y. Chen, L. Liu, P. Tao, M. P. Fan, N. Xu, X. W. Shen and C. L. Yan, *Adv. Mater.*, 2017, **29**, 1702268.

3 C. Liu, N. Xiao, H. J. Li, Q. Dong, Y. W. Wang, H. Q. Li, S. F. Wang, X. Y. Zhang and J. S. Qiu, *Chem. Eng. J.*, 2020, **382**, 121759.

4 M. Moussa, S. A. Al-Bataineh, D. Losic and D. P. Dubal, *Appl. Mater. Today*, 2019, **16**, 425-434.

5 B. J. Yang, J. T. Chen, L. Y. Liu, P. J. Ma, B. Liu, J. W. Lang, Y. Tang and X. B. Yan, *Energy Storage Mater*., 2019, **23**, 522-529.

6 Z. F. Li, W. Shin, Y. C. Chen, J. C. Neuefeind, P. A. Greaney and X. L. Ji, *ACS Appl. Energy Mater*., 2019, **2**, 4053-4058.

7 A. Mahmood, S. Li, Z. Ali, H. Tabassum, B. J. Zhu, Z. B. Liang, W. Meng, W. Aftab, W. H. Guo, H. Zhang, M. Yousaf, S. Gao, R. Q. Zou and Y. Y. Zhao, *Adv. Mater.*, 2019, **31**, 1805430.

8 H. H. Wang, G. Yang, Z. Chen, J. L. Liu, X. F. Fan, P. Liang, Y. Z. Huang, J. Y. Lin and Z. X. Shen, *J. Power Sources*, 2019, **419**, 82-90.

9 S. Jiang, Y. Li, Y. Qian, J. Zhou, T. Q. Li, N. Lin and Y. T. Qian, *J. Power Sources*, 2019, **436**, 226847.

10 L. F. Wang, S. J. Li, J. L. Li, S. Yan, X. Y. Zhang, D. H. Wei, Z. Xing, Q. C. Zhuang and Z. C. Ju, *Mater. Today Energy*, 2019, **13**, 195-204.

11 Y. Z. Liu, C. H. Yang, Q. C. Pan, Y. P. Li, G. Wang, X. Ou, F. H. Zheng, X. H. Xiong, M. L. Liu and Q. Y. Zhang, *J. Mater. Chem. A*, 2018, **6**, 15162-15169.

12 P. X. Xiong, X. X. Zhao and Y. H. Xu, *ChemSusChem*, 2018, **11**, 202-208.

13 Z. C. Ju, P. Z. Li, G. Y. Ma, Z. Xing, Q. C. Zhuang and Y. T. Qian, *Energy Storage Mater.*, 2018, **11**, 38-46.

14 X. D. He, J. Y. Liao, Z. F. Tang, L. N. Xiao, X. Ding, Q. Hu, Z. Y. Wen and C. H. Chen, *J. Power Sources*, 2018, **396**, 533-541.

15 L. Y. Liu, Z. F. Lin, J.-Y. Chane-Ching, H. Shao, P.-L. Taberna and P. Simon, *Energy Storage Mater.*, 2019, **19**, 306-313.

16 Z. L. Jian, S. Hwang, Z. F. Li, A. S. Hernandez, X. F. Wang, Z. Y. Xing, D. Su and X. L. Ji, *Adv. Funct. Mater.*, 2017, **27**, 1700324.

17 Z. C. Ju, S. Zhang, Z. Xing, Q. C. Zhuang, Y. H. Qiang and Y. T. Qian, *ACS Appl. Mater. Interfaces*, 2016, **8**, 20682-20690.

18 Y. H. Feng, S. H. Chen, J. Wang and B. G. Lu, *J. Energy Chem.*, 2020, **43**, 129-138.

19 Y. W. Luo, L. J. Liu, K. X. Lei, J. F. Shi, G. Xu, F. J. Li and J. Chen, *Chem. Sci.*, 2019, **10**, 2048-2052.

20 J. T. Chen, B. J. Yang, H. X. Li, P. J. Ma, J. W. Lang and X. B. Yan, *J. Mater. Chem. A*, 2019, **7**, 9247-9252.

21 W. D. Qiu, H. B. Xiao, Y. Li, X. H. Lu and Y. X. Tong, *Small*, 2019, **15**, 1901285.

22 S. Y. Dong, Z. F. Li, Z. Y. Xing, X. Y. Wu, X. L. Ji and X. G. Zhang, *ACS Appl.*

Mater. Interfaces, 2018, **10**, 15542-15547.

23 Z. Y. Zhang, M. L. Li, Y. Gao, Z. X. Wei, M. N. Zhang, C. Z. Wang, Y. Zeng, B. Zou, G. Chen and F. Du, *Adv. Funct. Mater.*, 2018, **28**, 1802684.

24 L. Fan, K. Lin, J. Wang, R. Ma and B. Lu, *Adv. Mater.*, 2018, **30**, 1800804.